ChemComm

COMMUNICATION

View Article Online
View Journal | View Issue

Cite this: *Chem. Commun.*, 2019, 55, 4166

Received 13th February 2019,
Accepted 8th March 2019

DOI: 10.1039/c9cc01269a

rsc.li/chemcomm

An unprecedented $\{Ni_{14}SiW_9\}$ hybrid polyoxometalate with high photocatalytic hydrogen evolution activity†

Grégoire Paille,‡[ab] Amandine Boulmier,‡[a] Alexandre Bensaid,[b] Minh-Huong Ha-Thi,[c] Thu-Trang Tran,[c] Thomas Pino,[c] Jérôme Marrot,[a] Eric Rivière,[d] Christopher H. Hendon,[e] Olivier Oms,[a] Maria Gomez-Mingot,[b] Marc Fontecave,[b] Caroline Mellot-Draznieks,[b] Anne Dolbecq[a] and Pierre Mialane *[a]

A unique polyoxometalate complex made up of a tetradecanuclear nickel bisphosphonate cluster capping a $\{SiW_9\}$ unit has been characterized. This stable compound exhibits a high hydrogen evolution reaction photocatalytic activity under visible light irradiation *via* a reductive quenching mechanism.

The photocatalytic activity of polyoxometalates (POMs) has been widely studied mainly due to their exceptional ability to perform photoinduced multi-electron reactions. Over the past decade, their relevance to both photooxidation (water oxidation, oxidation of organic pollutants, *etc.*) and photoreduction (reduction of metal cations, protons, *etc.*) reactions has been evidenced and studied with growing interest.[1] In the subfield of the hydrogen evolution reaction (HER), the activity of POMs assisted by co-catalysts (in particular platinum-based co-catalysts) has been well-investigated.[2] Nevertheless, very few systems incorporating only POMs and a photosensitizer (PS) have been found to be efficient for the reduction of protons. Noticeably, Izzet *et al.* reported in 2013 an elegant HER-active POM hybrid compound whereby two iridium complexes, playing the role of a visible-light PS, are covalently linked to a Dawson $[P_2W_{17}O_{61}]^{10-}$ unit, with a turn-over number (TON) of 41 after 7 days in homogeneous conditions.[3] Another covalently linked iridium/POM system, where an Anderson platform is decorated by two iridium complexes, was reported by the group of Streb, with a TON of 80 after one week.[4] In the meantime, the group of Hill evidenced that the TBA salt of $[(PW_9O_{34})_2Ni_4(H_2O)_2]^{10-}$ (TBA = tetrabutylammonium) tetranuclear Ni^{II} complex (noted TBA-$P_2W_{18}Ni_4$) produces H_2 with a TON of 6500 after one week in the presence of $[Ir(ppy)_2(dtbbpy)]^+$ as the PS (noted [Ir], with ppy = 2-phenylpyridine and dtbbpy = 4,4′-di-*tert*-butyl-2,2′-bipyridine) and triethanolamine (TEOA) as a sacrificial electron donor.[5] The catalytic activity of such fully inorganic multinuclear Ni^{II} polyoxotungstates has been recently confirmed,[6] while it has been shown that simple monosubstituted Ni^{II} Keggin POMs can also present an HER activity with $[Ru(bpy)_3]^{2+}$ (bpy = bipyridine) as the PS.[7] It thus appears that, even if some POMs incorporating other 3d centers (Fe^{III}, or Cu^{II})[8] or lanthanide cations[9] have been scarcely reported as HER complexes, Ni^{II} polyoxotungstates are particularly attractive HER photocatalysts.

During the last few years, some of us have shown that bisphosphonate (BP) ligands can structure solution-stable Ni^{II} polyoxotungstates, as exemplified by the characterization of the $[\{(B\text{-}PW_9O_{34})Ni_3(OH)(H_2O)_2(Ale)\}_2Ni]^{14-}$ (noted $P_2W_{18}Ni_7Ale_2$, with Ale = alendronate = $[O_3PC(C_3H_6NH_3)(O)PO_3]^{4-}$) sandwich-type complex where two $\{PW_9\}$ units encapsulate a heptanuclear $\{Ni_7(Ale)_2\}$ core.[10] Such species were shown to be highly stable in the 7–10 pH range, and derivatives with various organic groups or coordination complexes were further reported.[10,11] Herein, we show the richness of this BP POM chemistry, reporting on a novel complex where a $\{Ni^{II}_{14}\}$ fragment structured by Ale ligands caps a $\{SiW_9\}$ trivacant POM. To the best of our knowledge, such an arrangement is unique in POM chemistry, this compound constituting by far the polyoxotungstate with the highest 3d metal/tungsten atomic ratio reported to date. The HER activity of this functionalizable, high-nuclearity 3d system has been investigated in detail, highlighting the benefit of accumulating 3d centers on the photocatalytic properties.

$Na_{12}[(\alpha\text{-}A\text{-}SiW_9O_{34})Ni_{14}(AleH)_5(Ale)_2(H_2O)_{11}(OH)_7]\cdot 75H_2O$ (Na-$SiW_9Ni_{14}Ale_7$) was synthesized in water by heating at 80 °C a solution of nickel chloride, alendronic acid and $[\alpha\text{-}A\text{-}SiW_9O_{34}]^{10-}$ (SiW_9)

[a] *Institut Lavoisier de Versailles, UMR CNRS 8180, Université de Versailles Saint-Quentin en Yvelines, Université Paris-Saclay, 45 Avenue des Etats-Unis, 78035 Versailles Cedex, France. E-mail: pierre.mialane@uvsq.fr*
[b] *Laboratoire de Chimie des Processus Biologiques, UMR CNRS 8229, Collège de France, Sorbonne Université, PSL Research University, 11 Place Marcelin Berthelot, 75231 Paris Cedex 05, France*
[c] *Institut des Sciences Moléculaires d'Orsay (ISMO), CNRS, Univ. Paris-Sud, Université Paris-Saclay, F-91405 Orsay, France*
[d] *Institut de Chimie Moléculaire et des Matériaux d'Orsay, UMR 8182, CNRS, Univ. Paris-Sud, Université Paris-Saclay, 91405 Orsay cedex, France*
[e] *University of Oregon, Department of Chemistry and Biochemistry, Eugene, OR, 97403, USA*

† Electronic supplementary information (ESI) available. CCDC 1896611. For ESI and crystallographic data in CIF or other electronic format see DOI: 10.1039/c9cc01269a

‡ These authors contributed equally to this work.

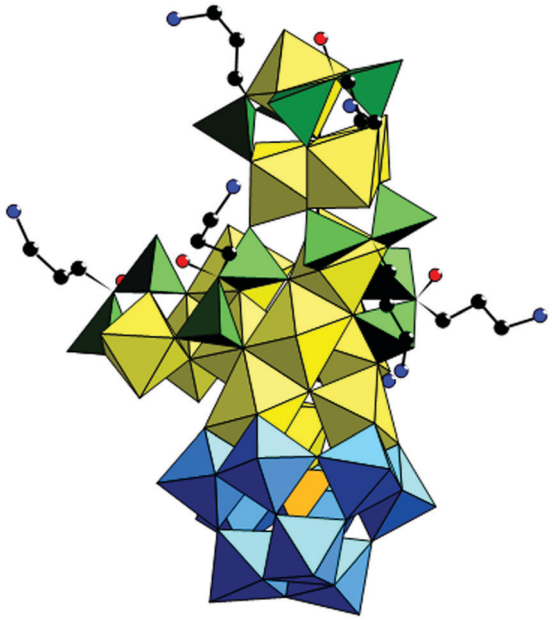

Fig. 1 Polyhedral and ball-and-stick representation of $SiW_9Ni_{14}Ale_7$; blue octahedra: WO_6, yellow octahedra: NiO_6, green tetrahedra: PO_3C, orange tetrahedron: SiO_4, black spheres: C, blue spheres: N, and red spheres: O. The hydrogen atoms have been omitted for clarity.

at a pH adjusted to 9.1 with sodium carbonate. The trivacant POM was used in excess, since attempts with the SiW_9 : Ni 1 : 14 stoichiometric ratio only afforded powders that we did not succeed in characterizing. After cooling the mixture at room temperature, a crystalline yellow powder slowly precipitated. Single-crystals of Na-$SiW_9Ni_{14}Ale_7$ were obtained by recrystallization in water. The single-crystal X-ray diffraction experiments (see Table S1, ESI,† for crystallographic data) showed that $SiW_9Ni_{14}Ale_7$ consists of a {α-A-SiW_9} unit capped by a tetradecanuclear Ni^{II} cluster which is structured by seven Ale ligands (Fig. 1). In addition, seven μ_3-hydroxo ligands (bond valence sum calculations = 0.94–1.13) ensure the cohesion of the {Ni_{14}} cluster. The paramagnetic centers complete their coordination spheres with a total of eleven terminal water molecules. Elemental analysis together with EDS measurements confirmed the composition of Na-$SiW_9Ni_{14}Ale_7$ (see ESI† for details). Magnetic measurements are also in agreement with the determined structure. The $\chi_M T$ product *vs.* T curve related to a crystalline sample of Na-$SiW_9Ni_{14}Ale_7$ is represented in Fig. S1, ESI.† First, a plateau is observed between 300 and 100 K, with a $\chi_M T$ value of 17.6 $cm^3\ mol^{-1}$ K corresponding to $g = 2.24$ considering fourteen $S = 1$ Ni^{II} non-interacting magnetic centers. The g value is in perfect agreement with that found for the $P_2W_{18}Ni_7Ale_2$ compound previously reported,[10] confirming the Ni : W ratio in Na-$SiW_9Ni_{14}Ale_7$. Below 100 K, the $\chi_M T$ product continuously decreases to 2 K ($\chi_M T$ = 2.5 $cm^3\ mol^{-1}$ K), indicating that in addition to magnetic anisotropy characterizing such $S = 1$ Ni^{II} ions, overall weak antiferromagnetic interactions are predominant. Considering both the high nuclearity and the C_1 symmetry of the {Ni_{14}} core, no attempt to fit the data with a Heisenberg Hamiltonian was performed. The IR spectrum of Na-$SiW_9Ni_{14}Ale_7$ (Fig. S2, ESI†) presents the typical vibrational bands of the SiW_9 fragment (990–670 cm^{-1}) and of the P–O groups of the Ale ligands (1050 cm^{-1}). The IR spectrum of a powder obtained by dissolution in water of Na-$SiW_9Ni_{14}Ale_7$ followed by the addition of NaCl is strictly similar to that of Na-$SiW_9Ni_{14}Ale_7$ (Fig. S2, ESI†), strongly suggesting that the title complex is stable in aqueous solution. Note that the IR spectrum of Na-$SiW_9Ni_{14}Ale_7$ is highly characteristic. The I_{W-O}/I_{BP} ratio (where I_{W-O} and I_{BP} stand for the intensity of the W–O and P–O vibrations, respectively) is indeed much higher for $SiW_9Ni_{14}Ale_7$ than for the other Ale/3d metal/polyoxotungstates previously reported, in agreement with a Ale : XW_9 (X = Si, and P) ratio of 7 : 1 in $SiW_9Ni_{14}Ale_7$, at variance with the 1 : 1 ratio reported for the earlier published compounds.[10–12] In addition, UV-Vis spectroscopy in aqueous solution revealed no significant variation over a period of 12 h of the Ni^{II} d–d transition bands characterizing $SiW_9Ni_{14}Ale_7$ (Fig. S3, ESI†). In order to obtain a derivative of $SiW_9Ni_{14}Ale_7$ soluble in organic solvents, metathesis of the sodium countercations with bis(triphenylphosphoranylidene)ammonium (P_2N) cations has been performed, affording the $(P_2NC_{36}H_{30})_8Na_4[(\alpha\text{-A-}SiW_9O_{34})Ni^{II}_{14}(AleOH)_5(AleO)_2(H_2O)_{11}(OH)_7]\cdot 60H_2O$ (P_2N-$SiW_9Ni_{14}Ale_7$) complex. The IR spectrum of the organo-soluble P_2N-$SiW_9Ni_{14}Ale_7$ clearly shows the bands characteristic of both the $SiW_9Ni_{14}Ale_7$ POM and the P_2N countercations (Fig. S4, ESI†). Its composition was further confirmed by elemental analysis and EDS measurements (see ESI† for details).

The HER catalytic activity of P_2N-$SiW_9Ni_{14}Ale_7$ was investigated in acetonitrile under visible light irradiation using [Ir] as PS, TEOA as a proton donor and 1-benzyl-1,4-dihydronicotinamide (BNAH) as the sacrificial electron donor. Various concentrations of the catalyst were investigated, from 5 to 60 μM. H_2 formation was monitored by gas chromatography. As shown in Fig. 2, upon irradiation, H_2 was formed immediately and its production increased with time up to a plateau, reached at various reaction times depending on the catalyst concentration: the larger the concentration, the later the plateau.

This is even better seen in Fig. S5 (ESI†) which translates the data of Fig. 2 into TON values as a function of time. We have established that this plateau is the result of the inactivation of the PS and not of the POM. Indeed, immediately after addition of a fresh solution of the [Ir] complex (final [Ir] concentration 200 μM) to the reaction medium after reaching the plateau, hydrogen production resumed with a rate similar to the initial

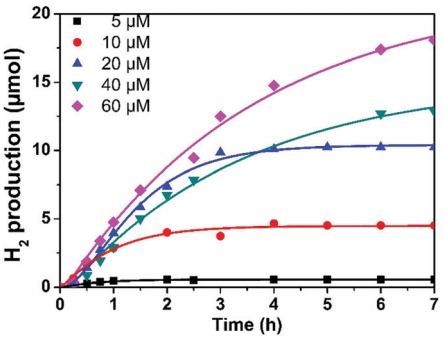

Fig. 2 Photocatalytic HER at different concentrations of P_2N-$SiW_9Ni_{14}Ale_7$. Conditions: xenon arc lamp (280 W, 415 < λ < 800 nm), [Ir] (0.2 mM), TEOA (0.25 M), BNAH (0.1 M), and 2 mL of CH_3CN deaerated with N_2.

one (Fig. S6, ESI†). As a further indication of the stability of the catalyst, the IR spectrum of the POM precipitated with $[Ru(bpy)_3]^{2+}$ from a postcatalytic solution after 4 h of illumination presents, together with the bands of the counter-cation, the characteristic signatures of $SiW_9Ni_{14}Ale_7$ (Fig. S7, ESI†). Based on the data of Fig. 2, the highest amount of H_2 (18 μmol after 7 h) was obtained with the most stable system (60 μM POM). However the highest initial TOF (turn-over frequency) values were obtained with 10–20 μM POM concentrations (2.7×10^{-2} s^{-1}) and the highest TON value was 256 for a concentration of 20 μM (Fig. S5, ESI†) after 4 h reaction. Compared in the same conditions, TBA-$P_2W_{18}Ni_4$ exhibited a TON of 41 after 4 h and an initial TOF of 9.8×10^{-3} s^{-1} (Fig. S8, ESI†).

To assess the contribution of each component to the photosystem, several control experiments were conducted. No hydrogen production could be detected in the absence of the catalyst or in the dark, and a negligible amount of hydrogen was measured when BNAH was removed or replaced with water (Fig. S9, ESI†). In addition, experiments using 14 equivalents of a Ni^{II} salt rather than the POM catalyst showed no catalytic activity (Fig. S9, ESI†). Furthermore, the addition of 150 mg of mercury to the reaction medium did not influence the production of hydrogen, showing that the active species is neither cationic nickel in solution nor Ni^0 nanoparticles, as also confirmed by DLS measurements.

Preliminary quantum chemical simulations were performed to elucidate the nature of the band edges in $SiW_9Ni_{14}Ale_7$ (computational details are provided in the ESI†). Owing to the low molecular symmetry of the polyoxometalate catalyst, there are numerous unoccupied frontier orbitals composed of hybrid W-d and Ni-d metal-centered orbitals. We present one of the LUMOs by projecting the electron density corresponding to the Kohn–Sham orbital equal to half the number of electrons +1, *i.e.* the first unoccupied molecular orbital, Fig. 3. Other LUMOs feature similar metal-d orbitals in various combinations. This unoccupied metal-d band is in good agreement with other transition metal-containing tungsten-based POMs[13] suggesting that here both W- and Ni-centers may participate in the HER.

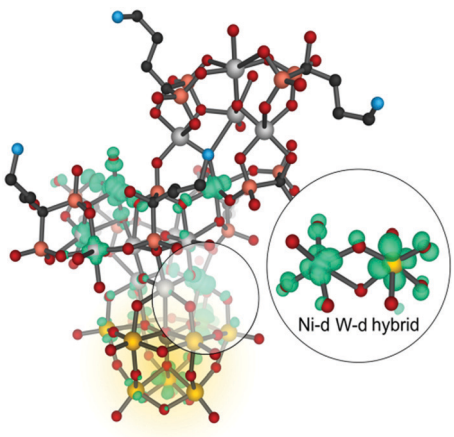

Fig. 3 One illustrative Frontier unoccupied orbital of $SiW_9Ni_{14}Ale_7$, composed of hybrid W-d and Ni-d orbitals. Electron density, shown in green, is drawn at 0.01 e^- $Å^{-3}$. Atoms depicted: W (yellow), Ni (light grey), Si (dark grey), C (black), O (red), N (blue), and P (orange).

In order to get insights into the reaction mechanism, time-resolved fluorescence measurements at 585 nm in CH_3CN solution containing 0.2 mM of [Ir] with increasing concentration of TEOA, BNAH or P_2N-$SiW_9Ni_{14}Ale_7$ and irradiated at 430 nm were then performed and analyzed according to the Stern–Volmer equation:

$$\tau_0/\tau = 1 + k_q\tau_0[Q]$$

where, τ_0 and τ are the emission lifetimes of [Ir] without and with the quencher Q of concentration [Q], respectively, and k_q is the quenching rate constant. The [Ir] complex indeed displays a broad emission with a maximum at 585 nm (Fig. S10, ESI†). From the data shown in Fig. 4 at concentrations used in the photochemical assay (yet lower for BNAH), photoluminescence lifetimes could be obtained (Table 1). Clearly, quenching rate constants in Table S2 (ESI†) deduced from the measurements at various concentrations of Q (Fig. S11, ESI†) indicated that under the conditions of the photocatalytic assay, the most efficient quenching of the emission was observed with BNAH. It results from this analysis that the reductive quenching of the PS is the dominant path.

The reductive quenching of [Ir]* by the sacrificial electron donor is further confirmed by transient absorption measurements. The transient absorption feature centered at 500 nm (Fig. S12, ESI†), assigned to the absorption of excited [Ir]*, decays following a mono-exponential law with a decay time of 520 ± 20 ns.

From decay times obtained in the presence of P_2N-$SiW_9Ni_{14}Ale_7$, TEOA or BNAH at the concentrations used in the photochemical assay (Fig. S13–S15, ESI†), it appears again that the fastest process is the electron transfer from BNAH to [Ir]*, leading to the reduced photosensitizer characterized by an absorption at 535 nm.[14] In short, the present system functions *via* a reductive quenching of the

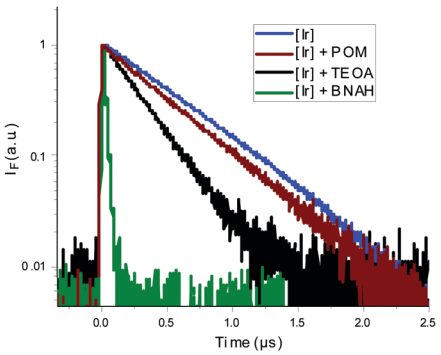

Fig. 4 Normalized time-resolved luminescence decays of [Ir] photosensitizer (0.2 mM), [Ir] with POM (20 μM), and [Ir] with TEOA (0.25 M) or BNAH (0.01 M) in CH_3CN (λ_{exc} = 430 nm).

Table 1 Photoluminescence lifetime of [Ir] photosensitizer (200 μM) in the presence of different quenchers: P_2N-$SiW_9Ni_{14}Ale_7$ (20 μM), TEOA (0.25 M) or BNAH (0.01 M) in CH_3CN (λ_{exc} = 430 nm)

	[Ir]	[Ir] + POM	[Ir] + TEOA	[Ir] + BNAH
Lifetime (ns)	520 ± 20	450 ± 20	260 ± 10	20 ± 10

PS, followed by reduction of the catalyst by the reduced PS. We can note that, under photocatalytic conditions, it has not been possible to evidence *via* UV-Vis spectroscopy the formation of reduced POM species, suggesting that the reduction of protons by the reduced POM is not the limiting step.

In summary, we reported herein on an unprecedented, stable POM where fourteen Ni^{II} centers cap a single trivacant Keggin unit. The organic/inorganic hybrid nature of this POM opens the way to the elaboration of a full family of derivatives, as already demonstrated for 3d bisphosphonate POMs in which the nitrogen atom of the Ale ligand has been functionalized by various organic or organometallic fragments.[10,11] While TBA-$P_2W_{18}Ni_4$ and P_2N-$SiW_9Ni_{14}Ale_7$ incorporate almost the same number of heavy atoms (22 and 23, respectively), a significantly higher HER activity was found for the title complex, suggesting that the accumulation of 3d centers in the POM core enhances the photocatalytic properties of such a complex. Time-resolved fluorescence together with transient absorption measurements suggest that during the photocatalytic process, the POM is reduced by the reduced photosensitizer. The immobilization of the reported species in matrices, which could lead to heterogeneous photocatalytic materials, is currently under study.

This work was supported by the Ministère de l'Enseignement Supérieur et de la Recherche, the CNRS, the Université de Versailles Saint Quentin en Yvelines and a public grant overseen by the French National Research Agency (ANR) as part of the "Investissements d'Avenir" program no. ANR-11-IDEX-0003-02 and CHARMMMAT ANR-11-LABX-0039. It used the Extreme Science and Engineering Discovery Environment (XSEDE), which is supported by National Science Foundation grant number ACI-1548562. CMD thanks GENCI (CINES/TGCC/IDRIS) for HPC resources through the grant 2016-097343.

Conflicts of interest

There are no conflicts to declare.

Notes and references

1 (*a*) S.-S. Wang and G.-Y. Yang, *Chem. Rev.*, 2015, **115**, 4893; (*b*) H. Lv, Y. V. Geletii, C. Zhao, J. W. Vickers, G. Zhu, Z. Luo, J. Song, T. Lian, D. G. Musaev and C. L. Hill, *Chem. Soc. Rev.*, 2012, **41**, 7572; (*c*) A. Dolbecq, P. Mialane, B. Keita and L. Nadjo, *J. Mater. Chem.*, 2012, **22**, 24509; (*d*) C. Streb, *Dalton Trans.*, 2012, **41**, 1651.

2 See for example: (*a*) J. Niu, F. Li, J. Zhao, P. Ma, D. Zhang, B. Bassil, U. Kortz and J. Wang, *Chem. – Eur. J.*, 2014, **20**, 9852; (*b*) Z. Y. Zhang, Q. P. Lin, S. T. Zheng, X. H. Bu and P. Y. Feng, *Chem. Commun.*, 2011, **47**, 3918; (*c*) K. Suzuki, F. Tang, Y. Kikukawa, K. Yamaguchi and N. Mizuno, *Angew. Chem., Int. Ed.*, 2014, **53**, 5356; (*d*) S. Li, S. Liu, S. Liu, Y. Liu, Q. Tang, Z. Shi, S. Ouyang and J. J. Ye, *J. Am. Chem. Soc.*, 2012, **134**, 19716.

3 B. Matt, J. Fize, J. Moussa, H. Amouri, A. Pereira, V. Artero, G. Izzet and A. Proust, *Energy Environ. Sci.*, 2013, **6**, 1504.

4 S. Shöweig, S. A. Rommel, J. Kübel, M. Micheel, B. Dietzek, S. Rau and C. Streb, *Chem. – Eur. J.*, 2016, **22**, 12002.

5 H. Lv, W. Guo, K. Wu, Z. Chen, J. Bacsa, D. G. Musaev, Y. V. Geletii, S. M. Lauinger, T. Lian and C. L. Hill, *J. Am. Chem. Soc.*, 2014, **136**, 14015.

6 (*a*) H. Lv, Y. Chi, J. van Leusen, P. Kögerler, Z. Chen, J. Bacsa, Y. V. Geletii, W. Guo, T. Lian and C. L. Hill, *Chem. – Eur. J.*, 2015, **21**, 17363; (*b*) X.-B. Han, C. Qin, X.-L. Wang, Y.-Z. Tan, X.-J. Zhao and E.-B. Wang, *Appl. Catal., B*, 2017, **211**, 349; (*c*) G.-H. Zhang, W.-B. Yang, W.-M. Wu, X.-Y. Wu, L. Zhang, X.-F. Kuang, S.-S. Wang and C.-Z. Lu, *J. Catal.*, 2019, **369**, 54.

7 K. von Allmen, R. Moré, R. Müller, J. Soriano-López, A. Linden and G. Patzke, *ChemPlusChem*, 2015, **80**, 1389.

8 (*a*) W.-C. Chen, C. Qin, X.-L. Wang, Y.-G. Li, H.-Y. Zhang, Y.-Q. Jiao, P. Huang, K.-Z. Shao, Z.-M. Su and E.-B. Wang, *Chem. Commun.*, 2014, **50**, 13265; (*b*) H. Lv, Y. Gao, W. Guo, S. Lauinger, Y. Chi, J. Bacsa, K. P. Sullivan, M. Wieliczko, D. G. Musaev and C. L. Hill, *Inorg. Chem.*, 2016, **55**, 6750.

9 M. A. Fashapoyeh, M. Mirzaei, H. Eshtiagh-Hosseini, A. Rajagopal, M. Lechner, R. Liu and C. Streb, *Chem. Commun.*, 2018, **54**, 10427.

10 H. El Moll, G. Rousseau, A. Dolbecq, O. Oms, J. Marrot, M. Haouas, F. Taulelle, E. Rivière, W. Wernsdorfer, D. Lachkar, E. Lacôte, B. Keita and P. Mialane, *Chem. – Eur. J.*, 2013, **19**, 6753.

11 G. Rousseau, S. Zhang, O. Oms, A. Dolbecq, J. Marrot, R. Liu, X. Shang, G. Zhang, B. Keita and P. Mialane, *Chem. – Eur. J.*, 2015, **21**, 12153.

12 (*a*) H. El Moll, A. Dolbecq, J. Marrot, G. Rousseau, M. Haouas, F. Taulelle, G. Rogez, W. Wernsdorfer, B. Keita and P. Mialane, *Chem. – Eur. J.*, 2012, **18**, 3845; (*b*) O. Oms, S. Yang, W. Salomon, J. Marrot, A. Dolbecq, E. Rivière, A. Bonnefont, L. Ruhlmann and P. Mialane, *Inorg. Chem.*, 2016, **55**, 1551.

13 (*a*) X. López, C. Bo and J. M. Poblet, *J. Am. Chem. Soc.*, 2002, **124**, 12574; (*b*) X. López, J. J. Carbó, C. Bo and J. M. Poblet, *Chem. Soc. Rev.*, 2012, **41**, 7537.

14 S. I. Bokarev, D. Hollmann, A. Pazidis, A. Neubauer, J. Radnik, O. Kühn, S. Lochbrunner, H. Junge, M. Beller and A. Brückner, *Phys. Chem. Chem. Phys.*, 2014, **16**, 4789.